

Vacuolar Nicotianamine Has Critical and Distinct Roles under Iron Deficiency and for Zinc Sequestration in *Arabidopsis*

Michael J. Haydon,^{a,b,c,1} Miki Kawachi,^{c,d,2} Markus Wirtz,^b Stefan Hillmer,^b Rüdiger Hell,^b and Ute Krämer^{a,b,c,3}

^aBioQuant Center, University of Heidelberg, D-69120 Heidelberg, Germany

^bCentre for Organismal Studies Heidelberg, University of Heidelberg, D-69120 Heidelberg, Germany

^cDepartment of Plant Physiology, Ruhr University Bochum, D-44801 Bochum, Germany

^dDepartment of Biology, Kobe University, Kobe 657-8501, Japan

The essential micronutrients Fe and Zn often limit plant growth but are toxic in excess. *Arabidopsis thaliana* ZINC-INDUCED FACILITATOR1 (ZIF1) is a vacuolar membrane major facilitator superfamily protein required for basal Zn tolerance. Here, we show that overexpression of ZIF1 enhances the partitioning into vacuoles of the low molecular mass metal chelator nicotianamine and leads to pronounced nicotianamine accumulation in roots, accompanied by vacuolar buildup of Zn. Heterologous ZIF1 protein localizes to vacuolar membranes and enhances nicotianamine contents of yeast cells engineered to synthesize nicotianamine, without complementing a Zn-hypersensitive mutant that additionally lacks vacuolar membrane Zn²⁺/H⁺ antiport activity. Retention in roots of Zn, but not of Fe, is enhanced in ZIF1 overexpressors at the expense of the shoots. Furthermore, these lines exhibit impaired intercellular Fe movement in leaves and constitutive Fe deficiency symptoms, thus phenocopying nicotianamine biosynthesis mutants. Hence, perturbing the subcellular distribution of the chelator nicotianamine has profound, yet distinct, effects on Zn and Fe with respect to their subcellular and interorgan partitioning. The *zif1* mutant is also hypersensitive to Fe deficiency, even in media lacking added Zn. Therefore, accurate levels of ZIF1 expression are critical for both Zn and Fe homeostasis. This will help to advance the biofortification of crops.

INTRODUCTION

Zn and Fe are essential micronutrients for all organisms, fulfilling critical structural and catalytic roles in a plethora of proteins in every aspect of metabolism and development (Vallee and Auld, 1990; Andreini et al., 2007). However, the very same powerful chemical properties that led to the selection of these transition metals for important biochemical functions can cause toxicity, and ultimately cell death, when these metals are present in excess (Fraústo da Silva and Williams, 2001). Consequently, despite a millimolar total requirement for cellular Zn in *Escherichia coli*, the amount of free Zn²⁺ was estimated at less than one cation per cell (Outten and O'Halloran, 2001). It is expected that this finding can be extrapolated to other transition metals and to cells of all organisms.

Fe deficiency is the most widespread micronutrient deficiency in humans, affecting more than 30% of the global population. Fe is a limiting nutrient to crop production, in particular on calcareous soils estimated to make up one-third of all agricultural soils

worldwide. This is a consequence of the low solubility of hydroxides and phosphates of ferric Fe that predominate in these soils (Palmer and Guerinot, 2009).

Plants possess tightly regulated and highly effective strategies for Fe acquisition and for controlling Fe movement within the plant (Palmer and Guerinot, 2009). However, these alone are not sufficient. Besides a shortage of Fe for metalloprotein functions under insufficient Fe supply, physiological Fe deficiency responses cause the accumulation of other transition metals, such as Zn and Cd. Therefore, mechanisms must exist to counteract simultaneously the deficiency of a target micronutrient and toxicities of secondary nontarget metals (Arrivault et al., 2006; Schaaf et al., 2006; Morrissey et al., 2009).

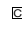
Metal homeostasis in plants requires tight and coordinated regulation of several classes of metal ion transport and metal trafficking proteins (Pilon et al., 2009), biosynthesis of various endogenous low molecular mass metal chelators (Callahan et al., 2006), and membrane transporters for chelators and metal-chelate complexes (Haydon and Cobbett, 2007a; Palmer and Guerinot, 2009). Nicotianamine (NA) is a low molecular mass metal chelator molecule with high binding affinity for a range of transition metal cations. It is synthesized enzymatically from three molecules of S-adenosyl Met by NICOTIANAMINE SYNTHASEs (NASs), which have been identified in vascular plants, *Neurospora crassa*, and *Archaea* and in silico in the moss *Physcomitrella patens* that was reported to contain NA (Higuchi et al., 1999; Trampczynska et al., 2006; Rensing et al., 2008; Dreyfus et al., 2009; Erxleben et al., 2012). The potential use of NA as an antihypertensive drug in humans is under study (Shimizu et al., 1999). Plants require NA to maintain phloem and cell-to-cell movement of Fe, and NA has also

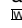
¹ Current address: Department of Plant Sciences, University of Cambridge, Downing Street, Cambridge CB2 3EA, United Kingdom.

² Current address: Graduate School of Bioagricultural Sciences, Nagoya University, Furo-cho, Nagoya 464-8601, Japan.

³ Address correspondence to ute.kraemer@rub.de.

The author responsible for distribution of materials integral to the findings presented in this article in accordance with the policy described in the Instructions for Authors (www.plantcell.org) is: Ute Krämer (ute.kraemer@rub.de).

 Some figures in this article are displayed in color online but in black and white in the print edition.

 Online version contains Web-only data.

www.plantcell.org/cgi/doi/10.1105/tpc.111.095042

been implicated in the symplastic movement of Zn and the transport of Cu in the xylem (Stephan and Scholz, 1993; Takahashi et al., 2003; Klatter et al., 2009; Trampczynska et al., 2010). Total tissue NA levels generally correlate with those of *NAS* transcripts, which are upregulated in response to Fe and Zn deficiencies and are constitutively high in Zn hyperaccumulator plants (Becher et al., 2004; Weber et al., 2004; Talke et al., 2006). Studies in heterologous systems showed that some YELLOW-STRIP1-LIKE (YSL) membrane transport proteins of the OLIGOPEPTIDE TRANSPORTER family can mediate the transport of metal-NA complexes into cells (Schaaf et al., 2004). YSLs of *Arabidopsis thaliana* have been implicated in the mobilization of Fe and other metals as NA complexes via the phloem during germination, leaf senescence, and seed loading (DiDonato et al., 2004; Le Jean et al., 2005; Waters et al., 2006; Chu et al., 2010).

Sequestration and storage of metals in vacuoles and their remobilization out of vacuoles are particularly important for plants to maintain cytosolic metal concentrations within a desired range during all developmental stages and metabolic states and to regulate the mobility of metals for subsequent long-distance transport (Lanquar et al., 2005, 2010; Kobae et al., 2004; Desbrosses-Fonrouge et al., 2005; Arrivault et al., 2006; Kim et al., 2006). Up to 80% of cellular Zn and ~50% of cellular Fe are sequestered within plant vacuoles (Lanquar et al., 2010). *A. thaliana* METAL TOLERANCE PROTEIN1 (MTP1) and MTP3 of the cation diffusion facilitator family are critical for transport of Zn²⁺ into vacuoles in shoots and roots, respectively (Kobae et al., 2004; Desbrosses-Fonrouge et al., 2005; Arrivault et al., 2006; Kawachi et al., 2008). VACUOLAR IRON TRANSPORTER1 and potentially also other members of the same protein family have an analogous role for Fe (Kim et al., 2006). ZINC-INDUCED FACILITATOR1 (ZIF1) was previously identified as a vacuolar membrane-localized major facilitator superfamily (MFS) transporter that is required for basal Zn tolerance in *A. thaliana* (Haydon and Cobbett, 2007b). It was proposed that ZIF1 might act in proton-coupled transport of a metal chelator or metal-chelate complex into vacuoles because the ZIF1 protein contains conserved motifs for proton/substrate antiport and related proteins mostly transport organic molecules.

In this article, evidence is provided that increasing the expression of *A. thaliana* ZIF1 is sufficient to raise the concentration of the endogenous metal chelator NA inside vacuoles, particularly in the root. We show that this promotes the vacuolar sequestration specifically of Zn, corroborating the previously described role of ZIF1 in basal Zn tolerance. In ZIF1-overexpressing plants, Zn is thus strikingly immobilized in roots, along with NA. Enhanced vacuolar sequestration of NA causes physiological NA deficiency in leaves. Accordingly, ZIF1 overexpressors exhibit reduced cell-to-cell mobility of Fe across the leaf blade and constitutive symptoms of Fe deficiency, very similar to biosynthetically NA-deficient plants. Not only ZIF1 overexpressors, but also *zif1* mutants, are hypersensitive to Fe deficiency, implying that accurate regulation of ZIF1 expression is critical for Fe homeostasis. Taken together, our results show that despite the lack of metal binding specificity of NA, through processes associated with ZIF1-dependent subcellular NA compartmentalization, *A. thaliana* achieves selective discrimination between Zn and Fe.

RESULTS

ZIF1 Affects Accumulation and Distribution of NA

Interveinal chlorosis is observed in leaves of transgenic lines strongly overexpressing ZIF1, and this is most severe in the youngest leaves (Figure 1A; see Supplemental Figure 1A online; Haydon and Cobbett, 2007b). This striking phenotype is reminiscent of NA-deficient plants (Stephan and Scholz, 1993; Takahashi et al., 2003; Klatter et al., 2009), suggesting that artificially enhanced ZIF1 activity causes cytoplasmic NA depletion. Therefore, NA was quantified by HPLC in leaves of soil-grown 35S-ZIF1-green fluorescent protein (GFP) (Haydon and Cobbett, 2007b) and wild-type plants. Contrary to the NA deficiency phenotype, total leaf NA concentrations were 1.7-fold higher in mature plants overexpressing ZIF1 than in the wild type (Figure 1B). To investigate this further, 35S-ZIF1-GFP, a newly identified 35S-ZIF1 line, the wild type, and *zif1-3* (Haydon and Cobbett, 2007b) were grown on agar media to determine both shoot and root NA concentrations. When grown on control media, roots of 35S-ZIF1-GFP and 35S-ZIF1 seedlings contained 14- and 28-fold higher levels of NA, respectively, than the wild type (Figure 1C). Upon growth on excess Zn or under Fe deficiency, expression of endogenous ZIF1 is known to increase (Haydon and Cobbett, 2007b; Yang et al., 2010), and root NA concentrations were 3.7- and 8.6-fold higher, respectively, in ZIF1 overexpressing lines than in wild-type plants (see Supplemental Figure 1 online). Although there was a tendency for *zif1-3* to contain lower NA concentrations than the wild type, this was not statistically significant. Further differences in shoot or root NA concentrations between the analyzed genotypes and the wild type were comparably minor. Increased root NA concentrations in 35S-ZIF1-GFP seedlings were accompanied by 2.3-fold higher total *NAS* transcript levels in comparison to the wild type, contributed primarily by *NAS2* (see Supplemental Figure 1F online).

Functional ZIF1-GFP was previously localized to the vacuolar membrane (Haydon and Cobbett, 2007b). The pronounced accumulation of NA in roots of ZIF1-overexpressing plants and the symptoms of cytoplasmic NA depletion in shoots observed here suggested a role for ZIF1 in enhancing the subcellular compartmentalization of NA into vacuoles. To test this hypothesis, transmission electron microscopy (TEM) was employed to detect immunogold-labeled NA in root tip cells of wild-type and 35S-ZIF1-GFP seedlings (Pich et al., 1997). On average, the number of gold particles per area (particle density) was threefold higher in images of 35S-ZIF1-GFP than wild-type cells (see Supplemental Figure 1G online). This is consistent with NA quantification in whole-root extracts of seedlings grown on media containing 30 μ M Zn, thus validating the detection of NA by this method (see Supplemental Figure 1C online). Furthermore, NA was detected predominantly inside vacuoles of 35S-ZIF1-GFP root cells, whereas in the wild type, NA was about equally abundant inside and outside of vacuoles (Figure 1D). Particle density within the vacuole relative to outside indicated an on average 3.6-fold higher proportion of vacuolar NA in 35S-ZIF1-GFP root cells than in the wild type (Figure 1E). By comparison, quantification of the number of gold particles in the

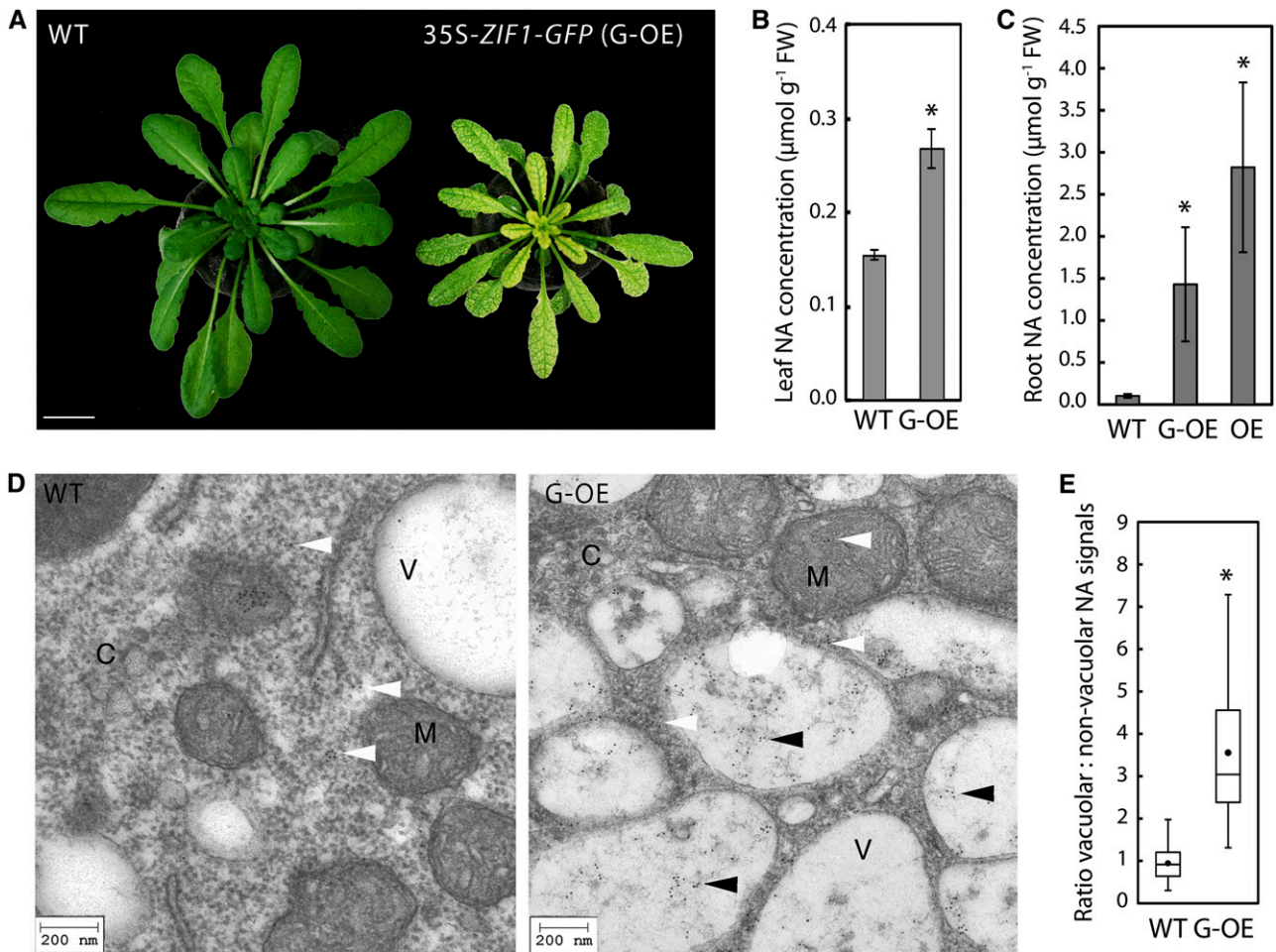


Figure 1. ZIF1 Enhances Vacuolar Sequestration of NA.

(A) Interveinal chlorosis of soil-grown 47-d-old 35S-ZIF1-GFP plants (G-OE; right) compared with the wild type (WT [Col]; left). Bar = 10 mm.

(B) Leaf NA concentrations of Col and 35S-ZIF1-GFP (mean \pm SD, $n = 4$) plants grown as in **(A)**. FW, fresh biomass.

(C) Root NA concentrations in 20-d-old Col, 35S-ZIF1-GFP, and 35S-ZIF1 (OE) (mean \pm SD, $n = 4$) seedlings grown on control medium.

(D) TEM images of immunogold-labeled NA in root tip cells of 21-d-old Col (left) and 35S-ZIF1-GFP (right) seedlings grown on medium containing $30 \mu\text{M}$ Zn. Cytosol (C), vacuoles (V), and mitochondria (M) are marked. Vacuolar and nonvacuolar gold particles are indicated by black and white arrowheads, respectively. Bars = 200 nm.

(E) Quantification of the subcellular distribution of immunogold-labeled NA in the wild type and G-OE. Gold particles inside and outside vacuoles were counted in TEM images, normalized to the respective area, and ratios were calculated. Boxes represent median, lower, and upper quartiles of $n = 19$ images per genotype (representative images shown in **(D)**); black dots are arithmetic means; error bars represent minima and maxima.

Asterisks denote significant differences from the wild type by Student's t test, with Bonferroni corrections ($P < 0.05$) in **(B)** and **(C)**, and by Mann-Whitney test ($P < 0.001$) in **(E)**.

[See online article for color version of this figure.]

mitochondria did not detect a significant difference between genotypes (on average 4.04 and 4.06 particles per mitochondria for the wild type and G-OE, respectively). Together, this supports the hypothesis that ZIF1 overexpression leads to enhanced sequestration of NA specifically inside vacuoles. In roots, this appears to trigger homeostatic mechanisms to enhance NAS gene expression and NA biosynthesis.

The increased vacuolar NA contents in root tips of 35S-ZIF1-GFP plants may be a direct effect or, alternatively, result from a compensatory response triggered by ZIF1-mediated changes in

A. thaliana metabolism or metal homeostasis. To obtain further evidence for the function of ZIF1 protein, a ZIF1 cDNA was expressed in the heterologous system *Saccharomyces cerevisiae*, which lacks endogenous NA biosynthesis. In wild-type yeast cells, ZIF1-GFP, GFP-ZIF1, and HA-ZIF1 all localized to internal, mostly vacuolar, membranes, as previously observed in *A. thaliana* (Figure 2A; see Supplemental Figure 2 online; Haydon and Cobbett, 2007b). Heterologous expression of *Arabidopsis halleri* NAS3 in yeast cells, which is known to confer increased Zn tolerance (Becher et al., 2004), led to ~ 60 -fold higher NA

contents than background detection limits of 0.062 ± 0.033 pmol 10^{-6} cells ($n = 3$) in wild-type yeast. Cotransformation of wild-type yeast with the Ah-NAS3 and *ZIF1* cDNAs gave rise to a 1.6-fold increase in NA content compared with yeast expressing Ah-NAS3 alone (Figure 2B). Taken together, these data suggest that *ZIF1* can enhance vacuolar NA accumulation when expressed in yeast.

Addition of 1 mM Zn to the media resulted in a further increase in total yeast NA content, with threefold higher NA levels in cells expressing *ZIF1* compared with empty-vector control transformants. By contrast, addition of 1 mM Fe to the medium did not affect NA contents of yeast cells expressing *ZIF1* (Figure 2B). Next, we tested the possibility that *ZIF1* transports a Zn-NA complex by examining whether *ZIF1* expression complements Zn hypersensitivity of a *zrc1 cot1* mutant. This mutant lacks the two vacuolar membrane transporters that contribute to Zn^{2+}/H^{+} antiport-mediated sequestration of Zn^{2+} in the vacuole (Simm et al., 2007). *ZIF1* failed to complement *zrc1 cot1*, with or without coexpression of Ah-NAS3 (Figure 2D). Furthermore, coexpression of *ZIF1* with Ah-NAS3 did not functionally complement a fourfold reduction in total cellular Zn content of *zrc1 cot1* compared with wild-type cells when cultured in 0.2 mM Zn (Figure 2C). These results obtained for *ZIF1* contrast the complementation of *zrc1 cot1* phenotypes by cDNAs encoding the plant vacuolar Zn^{2+} transporters MTP1, MTP3, or Ah-MTP1;3 (Figure 2D; Becher et al., 2004; Desbrosses-Fonrouge et al., 2005; Arrivault et al., 2006) and suggest that *ZIF1* alone cannot effect the vacuolar sequestration of cytoplasmic Zn or Zn-NA.

In a wild-type yeast background containing heterologous NA and functional vacuolar Zn^{2+} transporters, Zn content was slightly increased in *ZIF1*-expressing cells, yet by a magnitude corresponding to cellular NA content (cf. Figures 2B and 2C). These data are consistent with the possibility that, by affecting vacuolar NA accumulation, *ZIF1* can indirectly cause enhanced vacuolar Zn sequestration in yeast if endogenous Zn^{2+}/H^{+} antiport activity is present, which is similar to our observations in *A. thaliana* (see below).

Overexpression of *ZIF1* Enhances Root Vacuolar Zn Sequestration and Systemically Activates Zn Deficiency Responses

Loss of *ZIF1* function leads to Zn hypersensitivity (Haydon and Cobbett, 2007b). Therefore, *ZIF1* activity might influence the amount of Zn that can be sequestered inside the vacuole. To test this, the Zn-fluorophore Zinpyr-1 was used for confocal imaging of Zn in roots (Sinclair et al., 2007). Compared with the wild type, higher Zinpyr-1 fluorescence was observed in 35S-*ZIF1*, particularly in root tips (Figure 3A). Within root tips of 35S-*ZIF1*, strong fluorescence was observed inside the lumen of cells corresponding to the localization of cell vacuoles. By comparison, in wild-type cells, the fluorescence was much weaker and more diffuse (Figure 3A). Quantification of the fluorescent Zinpyr-1 Zn signal within 150 μ m of the root cap confirmed significantly higher signal intensities in 35S-*ZIF1* compared with the wild type (Figure 3B). Consistent with this, the Zn concentration in whole 35S-*ZIF1*-GFP and 35S-*ZIF1* roots was ~ 25 and 75% higher, respectively, than in the wild type (Figure 3C). Combined with a reduction in bulk shoot Zn concentrations by $\sim 40\%$ (Figure 3D), this amounted to two- to threefold higher root-to-shoot ratios of

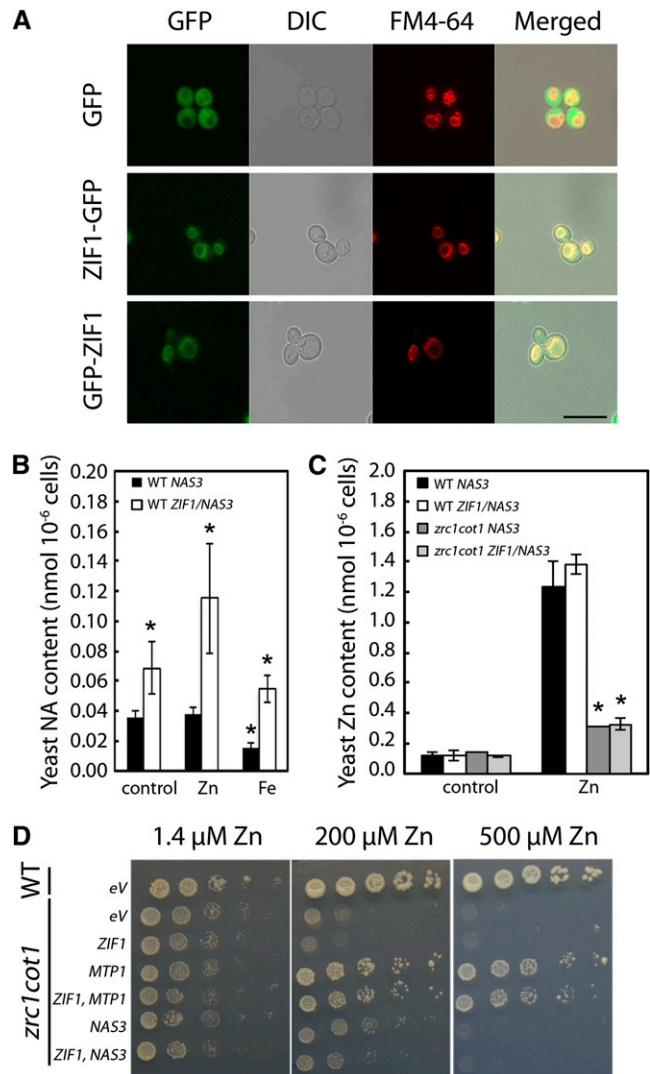


Figure 2. *ZIF1* Localizes to the Vacuole in Yeast and Enhances Accumulation of NA, but Not Zn.

(A) Confocal images of wild-type (BY4742) yeast transformed with empty vector (GFP), *ZIF1*-pUG35 (*ZIF1*-GFP), or *ZIF1*-pUG36 (GFP-*ZIF1*) cultured in SC-Ura-Met. GFP (green), differential interference contrast (DIC), the vacuole membrane marker dye FM4-64 (red), and merged images are shown. Bar = 10 μ m.

(B) NA concentrations in wild-type (WT) (BY4741) yeast cells transformed with either Ah-NAS3 alone or in combination with *ZIF1*, cultured in SC control medium, or supplemented with 1 mM $ZnSO_4$ or $FeSO_4$ (mean \pm SD, $n = 4$).

(C) Zn concentrations in the wild type or *zrc1 cot1* transformed with constructs as in **(A)** cultured in SC medium or SC medium supplemented with 200 μ M $ZnSO_4$ (mean \pm SD, $n = 3$).

(D) Growth of fivefold serial dilutions from $OD_{600} = 0.5$ cultures of the wild type (BY4741) or *zrc1 cot1* expressing *ZIF1*, or *ZIF1* in combination with At-MTP1 or Ah-NAS3, on LSP media containing 1.4, 200, or 500 μ M $ZnSO_4$. eV, empty vector.

Asterisks in **(B)** and **(C)** denote significant difference from wild-type NAS3 by Student's *t* test with Bonferroni corrections ($P < 0.05$).

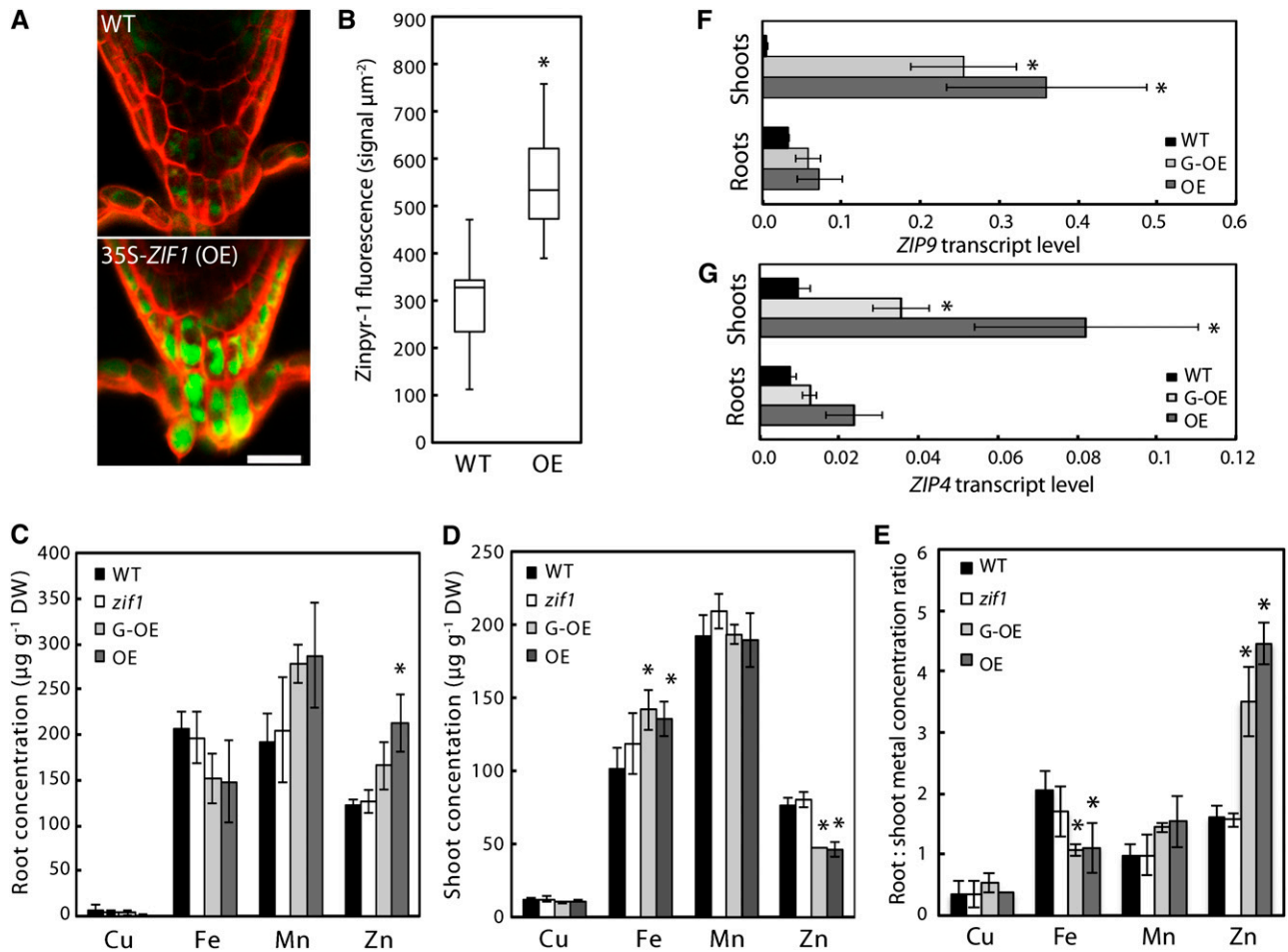


Figure 3. Promotion of Root Vacuolar Zn Sequestration through *ZIF1* Overexpression Activates Markers of Zn Deficiency.

(A) Confocal image of fluorescent Zn signals visualized using the Zn fluorophore Zinpyr-1 (green) in root tips of 10-d-old Col (wild type [WT]; top) and 35S-*ZIF1* (OE; bottom) seedlings grown on control media, counterstained with propidium iodide (red). Bar = 20 μm .

(B) Quantification of green fluorescent signal intensity within 150 μm of the root tip in the wild type and OE. Values are total intensities normalized to area; boxes represent median, lower, and upper quartiles of $n = 15$ images per genotype (representative images shown in **[A]**); error bars represent minima and maxima.

(C) to (E) Root **(C)** and shoot **(D)** concentrations and root:shoot concentration ratios **(E)** of Cu, Fe, Mn, and Zn in 20-d-old Col, *zif1-3*, 35S-*ZIF1*-GFP (G-OE), and 35S-*ZIF1* seedlings grown in control media, as determined by inductively coupled plasma atomic emission spectrometry (mean \pm SD, $n = 4$). DW, dry biomass.

(F) and (G) *ZIP9* **(F)** and *ZIP4* **(G)** transcript levels, relative to *UBQ10* and *ACT2*, in roots and shoots of 21-d-old Col, 35S-*ZIF1*-GFP and 35S-*ZIF1* seedlings grown on control media, determined by qRT-PCR (mean \pm SD, $n = 3$).

Asterisks denote significant difference from the wild type by Mann-Whitney test ($P < 0.001$) in **(B)** or by Student's *t* test ($P < 0.05$) with Bonferroni corrections in **(C)** to **(G)**.

Zn concentrations in both *ZIF1* overexpressing lines than in the wild type (Figure 3E). No such effect was apparent for other elements, including Fe, Mn, and Cu. By contrast, Fe concentrations were $\sim 35\%$ higher in shoots of *ZIF1*-overexpressing lines than in the wild type, and root-to-shoot Fe ratios were decreased by $\sim 50\%$ (Figures 3D and 3E). Relative transcript levels of the Zn deficiency marker genes *ZRT-*, *IRT-LIKE PROTEIN4* (*ZIP4*) and *ZIP9* were significantly higher in both roots and shoots of 35S-*ZIF1*-GFP seedlings than in the wild type (Figures 3F and 3G). These data are consistent with *ZIF1* functioning to promote the

sequestration of Zn inside vacuoles, thus removing it from the symplastic pathway of Zn movement across the root toward the xylem and the shoot.

***ZIF1* Is Transcriptionally Upregulated and Required in Fe-Deficient Plants and Can Modify the Intercellular Distribution of Fe**

Recent transcriptomic studies of Fe deficiency responses of *A. thaliana* revealed that *ZIF1* transcript levels are not only upregulated

in response to high Zn exposure (Haydon and Cobbett, 2007b) but also under Fe deficiency (Dinnyeny et al., 2008; Yang et al., 2010; Long et al., 2010). This was confirmed using a representative *ZIF1pGUS* (for β -glucuronidase) reporter line (Haydon and Cobbett, 2007b) for *ZIF1* promoter activity and by quantitative real-time RT-PCR (qRT-PCR; see Supplemental Figure 3 online; Figure 4A). The Fe-responsive transcriptional regulation of a gene encoding a transporter governing the subcellular distribution of Zn rather than Fe is intriguing. *A. thaliana* *MTP3* encodes a root vacuolar Zn^{2+}/H^{+} antiporter that is upregulated under Fe deficiency and excess Zn, similar to *ZIF1* (Arrivault et al., 2006; Haydon and Cobbett, 2007b). By mediating vacuolar Zn seques-

tration, *MTP3* was proposed to accommodate high rates of inadvertent Zn influx into the root symplasm, which arise from an increase in protein abundance of the high-affinity, but nonspecific root Fe uptake transporter IRON-REGULATED TRANSPORTER1 (IRT1) under Fe deficiency (Connolly et al., 2002; Vert et al., 2002; Arrivault et al., 2006). To test whether *ZIF1* transcript levels are upregulated in response to Fe deficiency directly or as a secondary effect of increased IRT1-mediated Zn accumulation, *ZIF1* transcript levels were determined in two constitutively Fe-deficient mutants: an *irt1* mutant (*pam25*; Varotto et al., 2002) that lacks functional IRT1 protein and associated Zn accumulation and the *ferric reductase defective3-1* (*frd3-1*) mutant (Rogers and Gueriot,

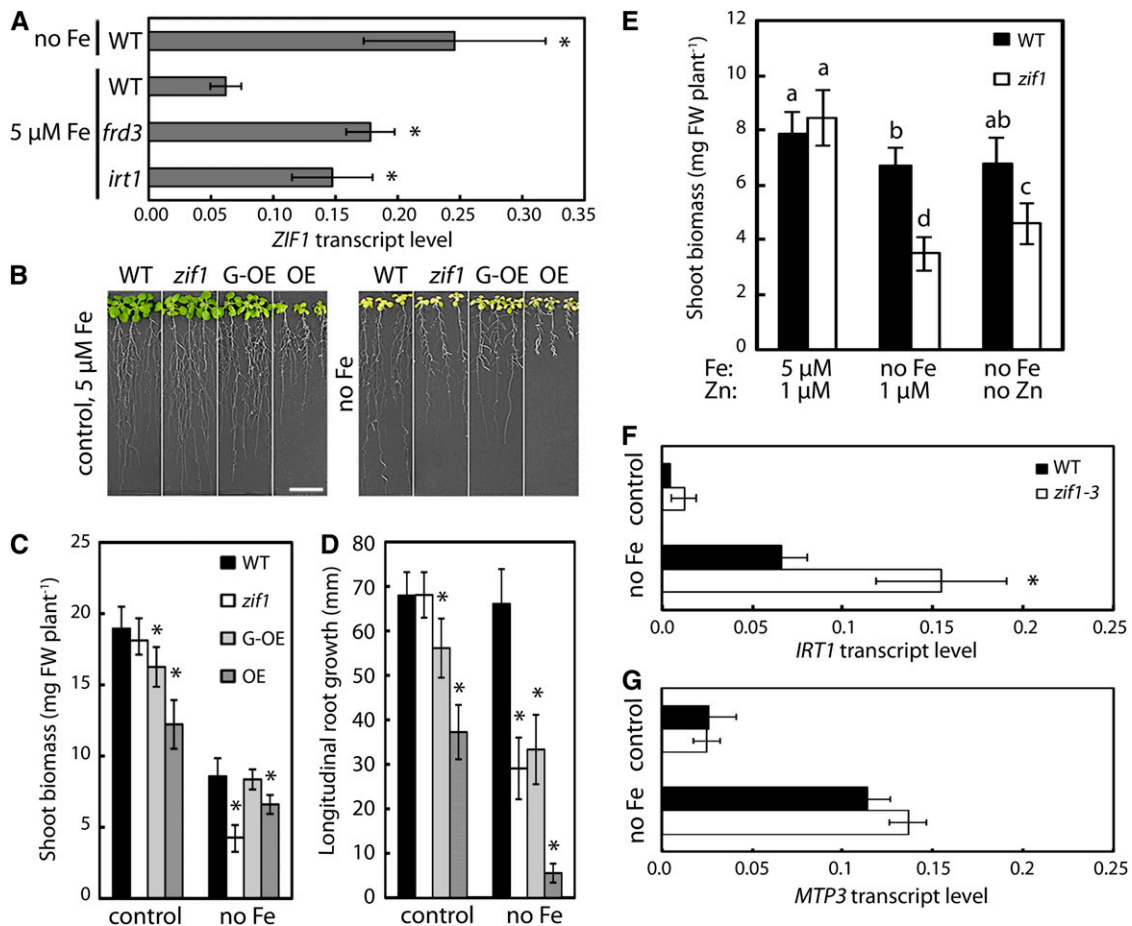


Figure 4. Loss of Function or Overexpression of *ZIF1* Are Both Detrimental to Plant Performance under Fe Deficiency.

(A) Transcript levels of *ZIF1*, relative to *UBQ10*, in shoots of 17-d-old Col (wild type (WT)), *frd3-1*, and *pam25* (*irt1*) seedlings grown on control media and the wild type grown on Fe-deficient (no Fe) media for 7 d, determined by qRT-PCR (mean \pm SD, $n = 3$).

(B) to (D) Photographs (B), shoot biomass (C), and root growth (D) of 17-d-old Col, *zif1-3*, 35S-*ZIF1*-GFP (G-OE), and 35S-*ZIF1* (OE) seedlings after 7 d growth on control or Fe-deficient (no Fe) media (mean \pm SE, $n = 4$). FW, fresh biomass. Bar = 10 mm.

(E) Shoot biomass of 17-d-old Col and *zif1-3* seedlings after 7 d growth on control or Fe-deficient (no Fe) media with or without 1 μ M Zn (mean \pm SE, $n = 3$).

(F) and (G) *IRT1* (F) and *MTP3* (G) transcript levels, relative to *UBQ10* and *ACT2*, in roots of 14-d-old Col and *zif1-3* seedlings grown on control media or Fe-deficient media for 3 d, determined by qRT-PCR (mean \pm SD, $n = 3$).

Asterisks denote significant differences from the wild type in (A), (C), (D), (F), and (G), and different letters (E) denote pairwise differences, by Student's *t* test ($P < 0.05$) with Bonferroni corrections.

[See online article for color version of this figure.]

2002), in which functional IRT1 protein and thus Zn accumulation are constitutively present (see Supplemental Figures 3C and 3D online). Compared with the wild type, *ZIF1* transcript abundance was elevated in shoots of both the *irt1* and the *frd3* mutant to levels approximating Fe-deficient wild-type seedlings (Figure 4A). By contrast, *MTP3* transcripts levels were equivalent in *irt1* and Fe-sufficient wild-type roots (see Supplemental Figure 3 online). Despite their constitutive Fe deficiency, *irt1* mutants lack IRT1-dependent Zn accumulation and thus contain shoot Zn concentrations comparable to the wild type (see Supplemental Figure 3 online; Vert et al., 2002). Consequently, this result suggests a direct transcriptional upregulation of *ZIF1* transcript levels in response to Fe deficiency, whereas the upregulation of *MTP3* transcript levels in Fe-deficient seedlings appears to be indirect and triggered by excess Zn.

To address whether *ZIF1* is important for plant performance under Fe deficiency, *zif1-3* and *ZIF1* overexpressors were grown on Fe-deficient media (Figure 4B). Compared to the wild type, overexpression of *ZIF1* led to interveinal chlorosis and reduced biomass production and root growth on control media, whereas *zif1* mutants grew normally, as reported previously (Haydon and Cobbett, 2007b). On Fe-deficient media, however, both shoot biomass and root growth of *zif1-3* were dramatically reduced to ~50 and 43% of the wild type, respectively (Figures 4B to 4D). Furthermore, root growth of the *ZIF1* overexpressor lines was also strongly reduced on Fe-deficient media to ~50 and 8% of the wild type. This shows that correct regulation of *ZIF1* transcript levels is critical for normal growth of *A. thaliana* under Fe-deficient conditions. Next, it was tested whether *ZIF1* has an additional role under Fe deficiency, independent of its known role in Zn detoxification (Haydon and Cobbett, 2007b). Omission of Zn from the media suppressed the growth defect of Fe-deficient *zif1-3* partially, but not completely (Figure 4E). Furthermore, upon growth on Fe-deficient media, roots of *zif1-3* contained higher transcript levels than the wild type of the Fe deficiency marker gene *IRT1*, but interestingly not of the Zn excess marker gene *MTP3* (Figures 4F and 4G). These results are consistent with a direct role for *ZIF1* in plant growth under Fe deficiency, additional to its established role in basal Zn tolerance.

To investigate how *ZIF1* can affect Fe homeostasis, the *ZIF1* overexpressors were examined further. Interveinal chlorosis in transgenic tobacco (*Nicotiana tabacum*) lacking NA was previously associated with impaired movement of Fe from the leaf vasculature into the leaf blade (Takahashi et al., 2003). Perls' stain was used to detect ferric Fe localization in leaves of 35S-*ZIF1-GFP*. Staining was not visible in wild-type leaves, whereas blue staining indicated the accumulation of Fe in the vasculature of leaves of the *ZIF1*-overexpressing line (Figure 5A). A similar pattern of ferric Fe staining was also observed in 35S-*ZIF1* leaves. Root surface ferric-chelate reductase activity, which is required for Fe uptake in *A. thaliana* and is an established Fe deficiency marker, was higher in 35S-*ZIF1-GFP* plants than in the wild type when grown on control media (Figure 5B). Similarly, Fe deficiency-induced *IRT1* and *FERRIC REDUCTASE OXIDASE3* (*FRO3*) transcript levels were higher in 35S-*ZIF1-GFP* roots and shoots, respectively, compared with the wild type (Figures 5C and 5D), whereas transcript levels of Cu deficiency-inducible *FRO5* were similar in both genotypes (see Supplemental Figure 4

online; Bernal et al., 2012). Together, these data suggest that impaired intercellular Fe distribution in *ZIF1*-overexpressing lines causes systemic Fe deficiency. To confirm this, 35S-*ZIF1-GFP* and wild-type plants were supplemented with Fe, Zn, or both by foliar spray. Spraying with Fe suppressed chlorosis and growth defects in 35S-*ZIF1-GFP*, confirmed by chlorophyll content (Figures 5E and 5F) and shoot biomass measurements (Figure 5G). Biomass of 35S-*ZIF1-GFP* was slightly increased when sprayed with both Zn and Fe, compared with Fe alone. This demonstrates that the growth phenotypes of plants overexpressing *ZIF1* are predominantly a consequence of systemic Fe deficiency resulting from defects in intercellular Fe mobility, with Zn deficiency making a smaller contribution.

DISCUSSION

ZIF1 Overexpression Affects the Subcellular Distribution of NA and Causes Systemic Fe Deficiency

A. thaliana *ZIF1* was proposed to act as a membrane transporter of a Zn chelator or Zn-chelate into vacuoles important for basal Zn tolerance (Haydon and Cobbett, 2007b). Leaves of *ZIF1* overexpressors exhibit pronounced interveinal chlorosis (Haydon and Cobbett, 2007b; Figure 1A), similar to mutant or transgenic plants with severely reduced levels of the high-affinity low molecular mass metal chelator NA (Stephan and Scholz, 1993; Takahashi et al., 2003; Klatter et al., 2009). Vascular Fe accumulation, constitutive activation of physiological Fe deficiency markers, and amelioration by spraying with Fe are further hallmarks of NA-deficient plants found in *ZIF1* overexpressors (Figure 5). Consistent with a defect in intercellular Fe mobility of NA-deficient plants, *ZIF1* overexpressors exhibit higher total shoot Fe concentrations than the wild type (Figure 3D). However, contrary to NA-deficient genotypes, total tissue NA concentrations in *ZIF1* overexpressors are comparable to and progressively higher than in the wild type in shoots and extraordinarily high in roots. Localization of NA in *A. thaliana* root tips by immunogold electron microscopy suggested that *ZIF1* overexpression increases the amount and proportion of cellular NA localized inside vacuoles (Figure 1). Taken together, these results suggest that in *A. thaliana*, *ZIF1* overexpression causes defects in the intercellular mobility of Fe as a consequence of a depletion of cytoplasmic NA availability through enhanced NA sequestration inside vacuoles. Cytoplasmic NA depletion is likely to affect shoot tissues more severely because shoots of *ZIF1* overexpressors do not exhibit the pronounced compensatory upregulation of both *NAS* transcript and NA levels that is observed in roots.

Physiological Role of Vacuolar NA Sequestration

Enhancement of vacuolar partitioning of NA through increasing *ZIF1* expression levels has profoundly distinct effects on the distribution of Zn and Fe throughout the plant (Figure 3). Overexpression of *ZIF1* leads to Zn accumulation in root vacuoles. This is associated with increased root and reduced shoot Zn concentrations and with the transcriptional activation of Zn

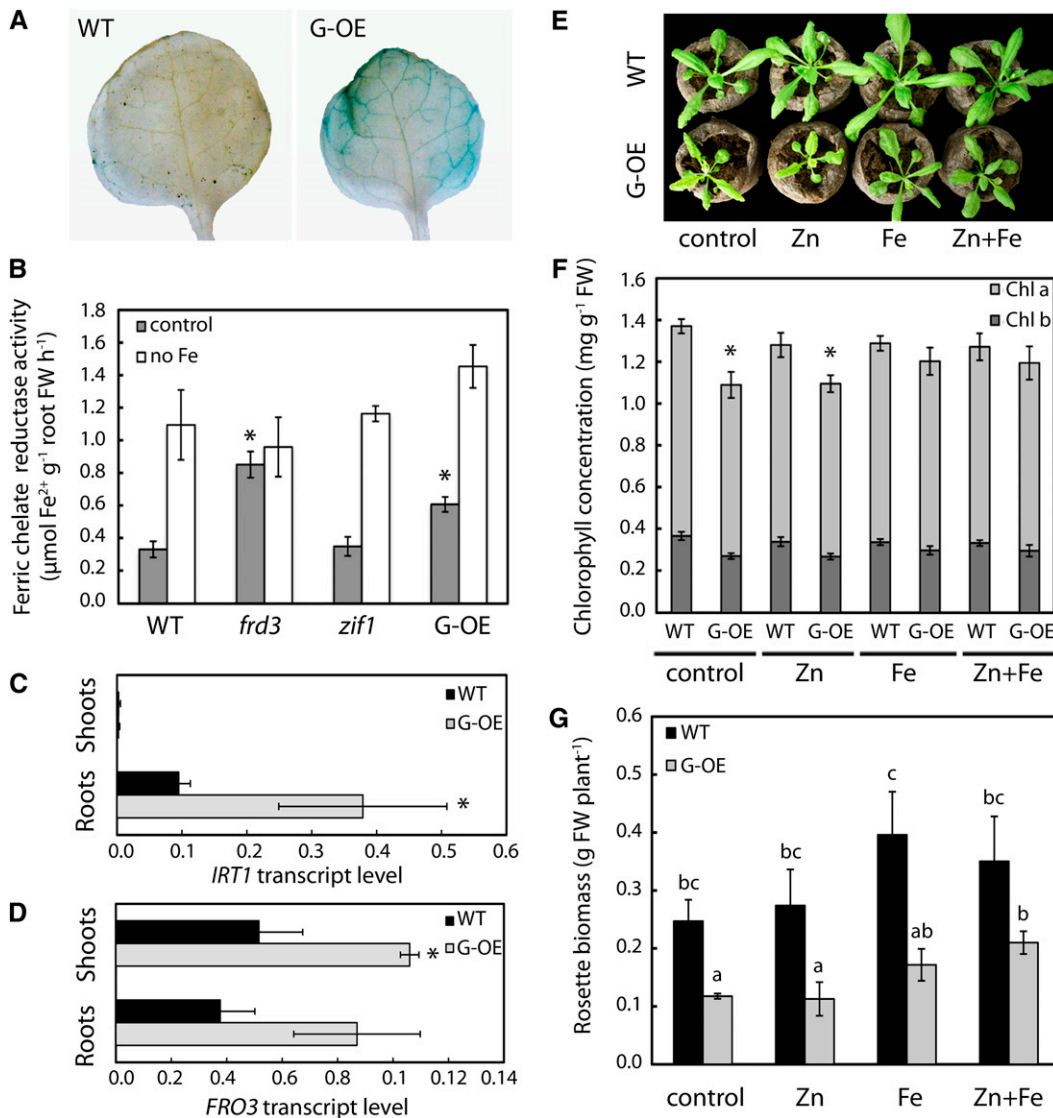


Figure 5. Fe Homeostasis Defects of *ZIF1*-Overexpressing Plants.

(A) Perls' stain for ferric Fe in Col (wild type [WT]) and 35S-*ZIF1-GFP* (G-OE) leaves of 35-d-old soil-grown plants.

(B) Root surface ferric-chelate reductase activity of 17-d-old Col, *frd3-1*, *zif1-3*, and 35S-*ZIF1-GFP* seedlings after 7 d growth on control or Fe-deficient (no Fe) media (mean \pm SD, $n = 4$). FW, fresh biomass.

(C) and (D) *IRT1* (C) and *FRO3* (D) transcript levels, relative to *UBQ10*, in shoots and roots of 21-d-old Col and 35S-*ZIF1-GFP* seedlings grown on control media, determined by qRT-PCR (mean \pm SD, $n = 3$).

(E) to (G) Photographs (E), leaf chlorophyll concentration (F), and shoot biomass (G) of soil-grown 27-d-old Col and 35S-*ZIF1-GFP* plants after 2 weeks of spraying with control (0.05% [v/v] Tween 20), 1 mM ZnSO_4 , and/or 0.5 g L^{-1} Fe-EDDHA every 3 to 4 d (mean \pm SD, $n = 4$).

Asterisks in (B) to (D) and (F) denote significant difference from the wild type by Student's *t* test with Bonferroni corrections ($P < 0.05$). Different letters in (G) indicate pairwise significant differences by Student's *t* test with Bonferroni corrections ($P < 0.05$).

deficiency responses confirming a reduction in internal Zn availability, particularly in shoots (Figure 3). These results are consistent with elevated cytosolic free Zn^{2+} concentrations in *zif1* mutants and explain the previously described mutant phenotypes (i.e., Zn hypersensitivity, enhanced shoot Zn accumulation, and the partial suppression of Zn deficiency phenotypes of the *hma2 hma4* double mutant impaired in root-to-shoot Zn trans-

location) (Hussain et al., 2004; Haydon and Cobbett, 2007b). By inference, our data suggest that reduced vacuolar NA concentrations render *zif1* mutants unable to sequester Zn effectively inside root vacuoles. Alternatively or additionally, elevated cytosolic availability of NA in *zif1* roots could promote Zn-NA complex formation that is predicted to enhance the mobility of Zn in the root symplasm, thus accelerating Zn passage to the xylem and

flux into aerial tissues (Lee et al., 2009), which are most sensitive to excess Zn.

Whereas root-to-shoot movement of Zn was reduced in *ZIF1* overexpressors, root-to-shoot translocation of Fe was not impaired (Figure 3E). This is similar to *nas* mutants of *A. thaliana* (Klatte et al., 2009). Instead, shoot Fe concentrations were higher in *ZIF1* overexpressors, suggesting an increased overall efficiency of root-to-shoot Fe translocation, contrasting the effect on root-to-shoot Zn mobility (Figure 3E; see Supplemental Figure 5 online). Additionally, the impaired intercellular Fe distribution in leaves of *ZIF1* overexpressors and the correction of interveinal chlorosis with Fe (Figure 5) are consistent with an important effect of ZIF1-dependent subcellular NA compartmentalization on other aspects of Fe homeostasis. Although the accumulation of Fe in vacuoles of the *ZIF1* overexpressing lines was not quantified, the lack of Fe accumulation in bulk root tissues argues against vacuolar Fe accumulation, different from Zn. The impaired Fe distribution in leaves of *ZIF1* overexpressors might be due to a dependence on the cytoplasmic formation of Fe-NA complexes for subsequent intra- and intercellular Fe transport, for example, in the phloem and via other membrane transporters, such as YSL proteins.

Despite a high affinity of NA for Cu (Callahan et al., 2006), no effects on Cu homeostasis were observed in the *ZIF1* overexpressing lines (Figure 3; see Supplemental Figure 4 online). This is similar to *nas* mutants (Klatte et al., 2009) and suggests that vacuolar NA does not impact significantly on Cu distribution in *A. thaliana*. However, since plants require Cu at much lower concentrations than Fe, a reduction of available NA might cause detectable defects in Cu accumulation only late in development or under specific growth conditions.

In combination, the regulation of *ZIF1* transcript levels and alterations in metal homeostasis of overexpressors and loss-of-function mutants suggest that ZIF1 has specific, yet distinct, roles in Zn and Fe homeostasis of *A. thaliana*. Thus, ZIF1 contributes to the establishment of metal specificity along the pathway of metal movement inside the plant subsequent to metal uptake.

***A. thaliana* Requires Balanced Regulation of *ZIF1* for Growth under Micronutrient Stress**

In mature vegetative tissues of wild-type plants, *ZIF1* is expressed at low levels in the vasculature, and promoter activity is strongly upregulated and more widely detected upon exposure to excess Zn (Haydon and Cobbett, 2007b) or Fe deficiency (see Supplemental Figure 3 online). The *zif1* mutant is hypersensitive to Fe deficiency, and this is partially reversed by further omission of Zn from the media (Figure 4). This confirms a role for ZIF1 in the detoxification of Zn when its influx is strongly enhanced under Zn excess and Fe deficiency, similar to the role proposed for MTP3 (Arrivault et al., 2006). However, this result also suggests that the function of ZIF1 under Fe deficiency is partly independent of its role in basal Zn tolerance and that ZIF1 functions in additional aspects of Fe homeostasis (see Supplemental Figure 5 online). The previous finding that *mtp1 zif1* double mutants are more sensitive to Zn excess than either of the two single mutants supports this, implying independent contributions of these vacuolar transporters to balancing micronutrient stress (Haydon and Cobbett, 2007b).

Furthermore, transcript levels of *ZIF1* are specifically upregulated in response to Fe deficiency, and this does not require secondary Zn accumulation occurring under Fe deficiency that, by contrast, triggers the upregulation of *MTP3* transcript levels (Figure 4; see Supplemental Figure 3E online).

The precise function of ZIF1 under Fe deficiency remains to be defined but might be to adjust cytosolic NA pools (see Supplemental Figure 5 online). For example, when NA biosynthesis is activated under Fe deficiency, ZIF1 might contribute to the dampening of temporal fluctuations in cytoplasmic NA concentrations or facilitate the mobilization of vacuolar Fe as an Fe-NA complex. Indeed, vacuole membrane proteomics identified YSL4 and YSL6 as candidates for the remobilization of metal-NA complexes from the vacuole into the cytoplasm (Jaquinod et al., 2007). Alternatively, by limiting the cytoplasmic accumulation of NA, ZIF1 might act to maintain cytoplasmic Fe availability to allow loading of cellular apo-metalloproteins or to restrict Fe export via the NA-dependent phloem transport pathway.

The recently described *popeye-1* (*pye-1*) mutant is hypersensitive to Fe deficiency (Long et al., 2010). Similar to *ZIF1*, *PYE* transcript levels are upregulated in response to Fe deficiency, yet it was reported that the *ZIF1* promoter is a direct target of negative regulation by the basic helix-loop-helix transcription factor PYE. Notably, under Fe deficiency, *ZIF1* transcript levels are upregulated to higher levels in *pye-1* than in wild-type seedlings (Long et al., 2010). Thus, it appears that PYE limits the extent of the increase in *ZIF1* transcript levels triggered under Fe deficiency. Consistent with this, *ZIF1* overexpressors grow poorly in Fe-deficient media (Figures 4 and 5).

Cellular Function of *ZIF1*

Previously characterized NA transporters are YSL proteins that import metal-NA complexes into the cell (Schaaf et al., 2004; DiDonato et al., 2004; Le Jean et al., 2005; Waters et al., 2006; Chu et al., 2010). Although direct biochemical evidence of ZIF1 transport function remains to be shown, we propose that ZIF1 is most likely to act as a transporter of free NA from the cytosol into the vacuole. This hypothesis is supported by the results obtained in Ah-NAS3-expressing yeast cells coexpressing *At-ZIF1*. Heterologous ZIF1 localized to the vacuolar membrane and caused an increase in cellular NA accumulation in wild-type yeast cells. *S. cerevisiae* lacks an endogenous NAS, making it unable to synthesize NA from S-adenosyl Met. Consequently, yeast is also expected to lack an effective mechanism for the retrieval of NA from vacuoles. *ZIF1* complemented neither the Zn hypersensitivity nor the reduced Zn accumulation of the *zrc1 cot1* mutant impaired in the transport of Zn²⁺ into vacuoles (Figure 2; Simm et al., 2007). This suggests that ZIF1 alone cannot mediate the transport of Zn or Zn-NA into vacuoles of yeast cells.

Our working model implies that the observed accumulation of Zn inside vacuoles of root tips of *ZIF1*-overexpressing *A. thaliana* plants (Figure 3A) is a secondary consequence of changed subcellular NA partitioning in ZIF1 overexpressors. There are several possible ways in which this may operate. It is possible that increased vacuolar NA concentrations promote the accumulation of Zn by mediating its chelation inside the vacuole.

Alternatively, the systemic Fe deficiency response detected in these lines could lead to an activation of IRT1-mediated Zn^{2+} uptake and vacuolar Zn^{2+} sequestration, for example, via MTP3 (Vert et al., 2002; Arrivault et al., 2006). However, expression of the corresponding genes is known to be specific to the more proximal root hair zone and not the root tip of wild-type roots. Finally, the depletion of cytoplasmic NA could trigger vacuolar Zn^{2+} sequestration. Comparisons between relative NA concentrations and the subcellular distribution of NA do not suggest a dramatic depletion of cytoplasmic NA in root tips of 35S-ZIF1-GFP plants (Figure 1E; see Supplemental Figures 1C and 1G online), but cytoplasmic NA depletion remains possible in the more mature regions of the root and is evident in leaves (Figures 1A and 1B; see Supplemental Figure 1F online). The reduced root-to-shoot transport of Zn in ZIF1-overexpressing lines can be explained by enhanced Zn sequestration in root vacuoles but is also consistent with a reduced shoot Zn content reported in *A. thaliana* NA-deficient *nas* mutants (Klatte et al., 2009). Wild-type seedlings and *nas* mutants were reported to be equally sensitive to toxic levels of Zn (Klatte et al., 2009), whereas ZIF1 overexpressors are Zn tolerant (Haydon and Cobbett, 2007b). This suggests that the overall effects of ZIF1 overexpression on root-shoot Zn partitioning might be attributable to a combination of a reduction in cytoplasmic and an increase in vacuolar availability of NA.

The finding that ZIF1 overexpression resulted in enhanced Zn content in root vacuoles and bulk root tissues of *A. thaliana* (Figure 3), but not strikingly in yeast cells (Figure 2), could be a consequence of only moderate ZIF1-dependent increases in NA contents in yeast when compared with *A. thaliana* roots (Figures 1C, 2B, and 2C). Our observation that ZIF1-dependent NA accumulation in wild-type yeast is enhanced by the addition of Zn, but not Fe (Figure 2B), might result from an activation of ZIF1 by Zn^{2+} or a dependence of NA accumulation on the formation of Zn-NA complexes inside the vacuole. It is possible that ZIF1 overexpression-associated vacuolar NA sequestration in root cells similarly depends on the transport of Zn^{2+} into the vacuole, for example, through MTP1 or MTP3 (Desbrosses-Fonrouge et al., 2005; Arrivault et al., 2006).

Metal complexes and precipitates inside vacuoles have been discussed as an important component of cellular metal tolerance, influencing the capacity and stability of vacuolar metal sequestration. As vacuolar chelators, phytochelatin, phytate, phosphate, and organic acid anions have received most attention to date (Callahan et al., 2006; Haydon and Cobbett, 2007a). Simulated models of metal chelation and experimental studies using electrospray ionization-mass spectrometry analysis of complexes formed in solution indicate that NA is able to chelate Zn^{2+} at vacuolar pH values (von Wirén et al., 1999; Rellán-Álvarez et al., 2008). By contrast, these studies suggest that Fe can be effectively chelated by NA in the cytoplasm, but not inside vacuoles. Thus, in general agreement with the observations reported here, high concentrations of NA are expected to sequester Zn more effectively than Fe inside plant vacuoles (see Supplemental Figure 5 online).

Recently, two proteins from rice (*Oryza sativa*), EFFLUX TRANSPORTER OF NA1 (ENA1) and ENA2, were reported to modestly enhance the efflux of radiolabel from *Xenopus laevis* oocytes injected with ^{14}C -NA (Nozoye et al., 2011). ENA2 en-

codes an ABC transporter-related protein, and ENA1 is an MFS protein that shares only 14% amino acid sequence identity with ZIF1 and is lacking sequence motifs common to all members of the ZIF1-LIKE (ZIFL) protein family (Ricachenevsky et al., 2011). This suggests that neither of the two transporters is related to ZIF1 or other plant ZIFL proteins. Similar to what is known for ZIF1, ENA1 is predicted to localize to the tonoplast, but the physiological functions of ENA1 and ENA2 proteins have not been described. It thus remains unclear what role these proteins might have in the accumulation or distribution of NA within rice plants (Nozoye et al., 2011).

A rice MFS protein, TRANSPORTER OF MUGINEIC ACID FAMILY PHYTOSIDEROPHORES1 (TOM1) shares 55% amino acid identity with ZIF1 and contains conserved motifs common to all members of the ZIFL family. TOM1 was concluded to mediate cellular efflux of the *Graminae*-specific NA-related Fe chelator deoxymugineic acid (DMA), but not NA, and to enhance DMA secretion from rice roots as the first step in Fe acquisition of this Strategy II plant (Nozoye et al., 2011). It was proposed that TOM1 transports free DMA. The ZIFL family is greatly expanded in grasses (Ricachenevsky et al., 2011), with TOM1 and 13 additional ZIFL genes encoded in the rice genome, compared with only three representatives in *A. thaliana*. Dicotyledonous plants such as *A. thaliana* do not synthesize DMA and related phytosiderophores derived from NA. It thus seems likely that different representatives of this plant-specific family of MFS transporters could exhibit differing specificities toward chemically related metal chelator molecules.

In summary, ZIF1 is a vacuolar membrane protein that contributes to the intracellular distribution of the low molecular mass metal chelator NA. This affects the partitioning of essential metals not only at the subcellular level, but also at the tissue and whole-plant levels, with remarkably distinct effects on Zn and Fe partitioning. Thus, the results presented here reveal a previously underappreciated role for vacuolar NA, first reported more than a decade ago (Pich et al., 1997), in plant metal homeostasis. Cell-specific expression of NAS genes successfully increased bioavailable concentrations of grain Zn and Fe in transgenic rice (Lee et al., 2009; Zheng et al., 2010). Coexpression of ZIF1 with NAS in cereal grains will be an attractive strategy to advance biofortification technologies.

METHODS

Plant Materials and Growth Conditions

Arabidopsis thaliana Columbia-0 was used as the wild type in all experiments. Mutants *zif1-3* (Haydon and Cobbett, 2007b), *frd3-1* (Rogers and Gueriot, 2002), and *irt1/pam25* (Varotto et al., 2002) and transgenic ZIF1pGUS line A10-6 and 35S-ZIF1-GFP line A3-1 (Haydon and Cobbett, 2007b) have been described. The 35S-ZIF1 line B2-1 is a homozygous T3 population identified from T2 that segregated 3:1 for the resistance marker, identified from a T1 population transformed with a previously described construct (Haydon and Cobbett, 2007b) by rescreening for DL-Phosphinothricin-resistant plants that displayed strong interveinal chlorosis.

For sterile plant culture, seeds were surface-sterilized for 10 min in 1.2% (v/v) NaOCl and 0.02% (v/v) Triton X-100, washed three times with sterile ultrapure water, and sown on modified Hoagland media containing

macronutrients (in mM) 1.5 Ca(NO₃)₂, 0.28 KH₂PO₄, 0.75 MgSO₄, and 1.25 KNO₃, micronutrients (in μM) 0.5 CuSO₄, 1 ZnSO₄, 5 MnSO₄, 25 H₃BO₃, 0.1 Na₂MoO₄, 50 KCl, and 5 Fe-HBED, buffered with 3 mM MES, pH 5.7, with 1% (w/v) Agar M (Sigma-Aldrich) and 1% (w/v) Suc in 12 × 12-cm square Petri plates. Seeds were placed at 4°C in the dark for 1 to 3 d and then grown vertically in 11 h light, 22°C/13 h dark, 18°C cycles. For Fe-deficient media, Agar M was washed three times with 50 mM EDTA, pH 5.7, for 8 to 16 h with continuous stirring, then washed six times with ultrapure water for at least 1 h and then used to prepare control media and media without Fe or Zn as indicated. For soil culture, seedlings were transferred to peat pellets (Jiffy) and grown in constant light or 8 h light 22°C/16 h 18°C dark (short day) cycles. Light was supplied at 100 to 150 μmol photons m⁻² s⁻¹.

Yeast Plasmids, Strains, and Growth

ZIF1 was amplified with Phusion DNA polymerase (Finnzymes) from Col-0 cDNA with forward primer 5'-CACCATGGCGGAGGAGTACA-3' and reverse primer 5'-TCATCTTCGACTCGTCTTAGAA-3' and cloned into pENTR-D/TOPO (Invitrogen) according to the manufacturer's instructions, then recombined into a Gateway-compatible pFL38H vector (Talke et al., 2006) using LR Clonase II (Invitrogen). Empty vectors pFL38 and pFL61 and/or *ZIF1*-pFL38H and *Ah-NAS3*-pFL61 (*Arabidopsis halleri* *NAS3* cDNA) (Becher et al., 2004) were cotransformed into *Saccharomyces cerevisiae* wild-type strain BY4741 (*Mat a*, *his3Δ1*, *leu2Δ0*, *met15Δ0*, *ura3Δ0*) and *zrc1cot1* (*Mat a*, *zrc1::natMX3*, *cot1::kanMX4*, *his3Δ1*, *leu2Δ0*, *met15Δ0*, *ura3Δ0*) (Becher et al., 2004) by the method described (Dohmen et al., 1991). Transformants were selected and maintained and experiments performed in synthetic complete (SC) media without His and Ura, with or without ZnSO₄ added as indicated.

For drop tests, yeast cultures were grown in triplicate to mid-log phase in low-sulphate phosphate (LSP) media (Talke et al., 2006) and diluted to OD₆₀₀ of 0.5. Fivefold serial dilutions were prepared in LSP, and 5 μL was dropped onto LSP media, solidified with 1.5% (w/v) agarose, with ZnSO₄ added as indicated. Plates were incubated at 30°C for 3 d.

For *ZIF1* localization in yeast, a *ZIF1* cDNA was amplified with forward primer 5'-AAGGAATTCATGGCGGAGGAGTACA-3' and either reverse primer 5'-AAGATCGATTCTTCGACTCGTCTTAGAAATG-3' or 5'-AAGATCGATTCTTCGACTCGTCTTAGAA-3' and cloned into *EcoRI* and *ClaI* restriction sites of pUG35 or pUG36 (Niedenthal et al., 1996), respectively. Transformants were cultured in SC without Ura, washed three times in sterile water, and resuspended in SC without Ura or Met at OD₆₀₀ = 0.1, and cultures were grown to OD₆₀₀ = 0.4. Cells were incubated in SC-Ura-Met with 40 μM FM4-64 for 20 min at 30°C, then washed with SC-Ura-Met and imaged by confocal microscopy. For immunoblots, vacuole membranes were prepared from BY4741 yeast transformed with *ZIF1*-pFL38H or pFL38 as previously described (Kawachi et al., 2008). Vacuole membrane proteins were denatured for 20 min at room temp in SDS loading buffer, separated by SDS-PAGE, and transferred to a polyvinylidene fluoride membrane. The membrane was probed with rabbit anti-HA antibody (Invitrogen) or anti-V-ATPase B (Invitrogen), then ECL anti-rabbit HRP-linked IgG (GE Healthcare), and chemiluminescence was detected with ECL Plus (GE Healthcare).

Measurement of Metals

For measurement of total metal concentrations, plant material was desorbed on ice with cold 5 mM CaSO₄, 1 mM MES, pH 5.7, for 10 min, cold 5 mM CaSO₄, 10 mM EDTA, 1 mM MES, pH 5.7, for 5 min, then washed twice with cold ultrapure water. For yeast, 10 mL of late log phase cultures was pelleted at 2100g at 4°C and washed three times with cold 10 mM CaCl₂ then twice with cold ultrapure water. Plant material and yeast pellets were dried at 60°C, digested in 2 mL 70% (v/v) HNO₃ at 90°C

for 4 h, followed by addition of 1 mL 30% (v/v) H₂O₂ and brief reheating and then diluted to 10 mL with ultrapure water. Metal concentrations were determined using an Iris Advantage Duo inductively coupled plasma atomic emission spectrometer (ThermoFisher).

Visualization of Zinpyr-1 (Sigma-Aldrich) in roots tips of 10-d-old seedlings grown on control media was performed after incubation for 1 h in 10 μM Zinpyr-1 as described (Sinclair et al., 2007). Roots were counterstained with propidium iodide (Sigma-Aldrich) and imaged with a Leica TCS SP5 confocal microscope (Leica Microsystems) using settings for fluorescein isothiocyanate and Texas Red with Argon laser power set to 30%, 488-nm excitation set to 30%, and gain at 800 V. Optical longitudinal sections were imaged through the center of the root, and total fluorescence in the fluorescein isothiocyanate channel was determined by measuring total signal as integrated density within 150 μm from the root tip using ImageJ software. Area of the root in each image was also calculated and used for normalization of the fluorescent signal. A total of 15 roots of each genotype from three independent experiments were imaged and analyzed.

Histochemical staining of ferric Fe was done by Perls' stain (Rogers and Gueriot, 2002).

Detection of NA

Frozen plant tissue (~60 mg) was ground in a ball mill (Retsch) at 30 orbits s⁻¹ for 1 min and extracted twice with 500 μL prewarmed (60°C) ultrapure water at 80°C with shaking at 500 rpm for 15 min. For yeast, 40 mL of late log phase liquid cultures were prepared as for metal measurements. Washed cell pellets were extracted in prewarmed (60°C) ultrapure water by lysis with an equal volume of glass beads in a ball mill (Retsch) at 30 orbits s⁻¹ for 3 × 1 min. Total NA concentration was determined in supernatants by HPLC as described (Klatte et al., 2009).

Immunogold Electron Microscopy

Immunogold localization of NA using an NA-specific antibody and TEM was performed as previously (Pich et al., 2001). Images were observed at 80 kV with a Jeol 1400 transmission electron microscope and captured with a Fastscan F214 digital camera (TVIPS). To determine the distribution of NA in root tip cells, gold particles inside and outside of vacuoles were counted in 19 images for each genotype and normalized to area using ImageJ software (National Institutes of Health).

Gene Expression Analysis

For qRT-PCR, total RNA was extracted from frozen plant tissue using an RNeasy plant mini kit (Qiagen), and cDNA was synthesized from 1 μg RNA with a RETROscript first-strand synthesis kit (Ambion) using oligo(dT) primer. Technical replicates of gene-specific products were amplified in 10-μL reactions using SYBR Green PCR Master Mix (Applied Biosystems) and the primers in Supplemental Table 1 online on an ABI Prism 7900 384-well real-time PCR machine (Applied Biosystems). Relative transcript levels were determined by incorporating PCR efficiencies as described (Talke et al., 2006) and normalizing to the geometric mean of expression of the reference gene(s) for each sample (Vandesompele et al., 2002).

To detect GUS expression, histochemical stains for GUS activity were done in whole seedlings of *ZIF1pGUS* transgenic lines for 16 h at 37°C as previously (Haydon and Cobbett, 2007b).

Spectrophotometric Assays

Root surface Fe(III)-chelate reductase assays were done as described (Yi and Gueriot, 1996) using whole roots of six to eight seedlings per replicate,

incubated in 1 mL assay buffer (0.3 mM ferrozine and 0.1 mM Fe-EDTA) for 20 min in the dark. Root tissue was blotted dry and fresh biomass was determined. Rates of Fe reductase activity were calculated using absorbance at 562 nm and a micromolar extinction coefficient of 28.6.

For determination of chlorophyll concentrations, rosette tissue was extracted with methanol at 70°C for 15 min with regular mixing. Absorbance was measured at 750, 665, 652, and 470 nm, and chlorophyll concentration was calculated as described (Porra et al., 1989).

Accession Numbers

Sequence data from this article can be found in the Arabidopsis Genome Initiative or GenBank/EMBL databases under the following accession numbers: *ZIF1*, At5g13740; *IRT1*, At4g19690; *FRD3*, At3g08040; *FRO3*, At1g23020; *ZIP4*, At1g10970; *ZIP9*, At4g33020; *FRO5*, At5g23990; *NAS1*, At5g04950; *NAS2*, At5g56080; *NAS3*, At1g09240; *NAS4*, At1g56430; *MTP3*, At3g58810; *ACT2*, At3g18780; *UBQ10*, At4g05320; and *Ah-NAS3*, AJ580399.

Supplemental Data

The following materials are available in the online version of this article.

Supplemental Figure 1. Effect of *ZIF1* Overexpression on NA Concentrations and *NAS* Transcript Levels.

Supplemental Figure 2. Detection of 3xHA-ZIF1 in the Vacuolar Membrane of Yeast.

Supplemental Figure 3. Fe-Dependent Regulation of *ZIF1* Promoter Activity and Transcript Levels.

Supplemental Figure 4. *ZIF1* Overexpressors Do Not Upregulate *FRO5*, a Transcriptional Marker of Cu Deficiency.

Supplemental Figure 5. Proposed Working Model for *ZIF1* Function under Micronutrient Stress.

Supplemental Table 1. Sequences of Primers Used for Quantitative Real-Time PCR.

ACKNOWLEDGMENTS

We thank Janine Specht and Petra Düchting for technical assistance. We thank Ralf Erdmann for pUG35 and pUG36, Dario Leister for *pam25*, and Mary Lou Guerinot for *fra3-1* seeds. We also thank Enrico Martinoia for useful comments and reading the manuscript. This research was funded by a European Union Marie Curie Fellowship to M.J.H. (PIIF-GA-2008-219457), by the European Union project "Public Health Impact of Long-Term, Low-Level Mixed Element Exposure in Susceptible Population Strata" (FOOD-CT-2006-016253), and the German Research Council (Deutsche Forschungsgemeinschaft; KR1967/4-1, 5-1) to U.K.

AUTHOR CONTRIBUTIONS

M.J.H. and U.K. designed the research. M.J.H., M.K., M.W., and S.H. performed experiments. R.H. contributed analytical tools. M.J.H., M.K., M.W., and U.K. analyzed data. M.J.H. and U.K. wrote and edited the article.

Received December 20, 2011; revised January 26, 2012; accepted February 9, 2012; published February 28, 2012.

REFERENCES

- Andreini, C., Banci, L., Bertini, I., Elmi, S., and Rosato, A. (2007). Non-heme iron through the three domains of life. *Proteins* **67**: 317–324.
- Arrivault, S., Senger, T., and Krämer, U. (2006). The Arabidopsis metal tolerance protein AtMTP3 maintains metal homeostasis by mediating Zn exclusion from the shoot under Fe deficiency and Zn oversupply. *Plant J.* **46**: 861–879.
- Becher, M., Talke, I.N., Krall, L., and Krämer, U. (2004). Cross-species microarray transcript profiling reveals high constitutive expression of metal homeostasis genes in shoots of the zinc hyperaccumulator *Arabidopsis halleri*. *Plant J.* **37**: 251–268.
- Bernal, M., Casero, D., Singh, V., Wilson, G.T., Grande, A., Yang, H., Dodani, S.C., Pellegrini, M., Huijser, P., Connolly, E.L., Merchant, S.S., and Krämer, U. (2012). Transcriptome sequencing identifies *SPL7*-regulated Cu acquisition genes *FRO4/FRO5* and the Cu dependence of Fe homeostasis in *Arabidopsis*. *Plant Cell* **24**: 738–761.
- Callahan, D.L., Baker, A.J., Kolev, S.D., and Wedd, A.G. (2006). Metal ion ligands in hyperaccumulating plants. *J. Biol. Inorg. Chem.* **11**: 2–12.
- Chu, H.H., Chiecko, J., Punshon, T., Lanzirrotti, A., Lahner, B., Salt, D.E., and Walker, E.L. (2010). Successful reproduction requires the function of Arabidopsis Yellow Stripe-Like1 and Yellow Stripe-Like3 metal-nicotianamine transporters in both vegetative and reproductive structures. *Plant Physiol.* **154**: 197–210.
- Connolly, E.L., Fett, J.P., and Guerinot, M.L. (2002). Expression of the *IRT1* metal transporter is controlled by metals at the levels of transcript and protein accumulation. *Plant Cell* **14**: 1347–1357.
- Desbrosses-Fonrouge, A.G., Voigt, K., Schröder, A., Arrivault, S., Thomine, S., and Krämer, U. (2005). *Arabidopsis thaliana* MTP1 is a Zn transporter in the vacuolar membrane which mediates Zn detoxification and drives leaf Zn accumulation. *FEBS Lett.* **579**: 4165–4174.
- DiDonato, R.J., Jr., Roberts, L.A., Sanderson, T., Easley, R.B., and Walker, E.L. (2004). Arabidopsis Yellow Stripe-Like2 (*YSL2*): A metal-regulated gene encoding a plasma membrane transporter of nicotianamine-metal complexes. *Plant J.* **39**: 403–414.
- Dinneny, J.R., Long, T.A., Wang, J.Y., Jung, J.W., Mace, D., Pointer, S., Barron, C., Brady, S.M., Schiefelbein, J., and Benfey, P.N. (2008). Cell identity mediates the response of Arabidopsis roots to abiotic stress. *Science* **320**: 942–945.
- Dohmen, R.J., Strasser, A.W., Höner, C.B., and Hollenberg, C.P. (1991). An efficient transformation procedure enabling long-term storage of competent cells of various yeast genera. *Yeast* **7**: 691–692.
- Dreyfus, C., Lemaire, D., Mari, S., Pignol, D., and Arnoux, P. (2009). Crystallographic snapshots of iterative substrate translocations during nicotianamine synthesis in Archaea. *Proc. Natl. Acad. Sci. USA* **106**: 16180–16184.
- Erxleben, A., Gessler, A., Vervliet-Scheebaum, M., and Reski, R. (2012). Metabolite profiling of the moss *Physcomitrella patens* reveals evolutionary conservation of osmoprotective substances. *Plant Cell Rep.* **31**: 427–436.
- Fraústo da Silva, J.J.R., and Williams, R.J.P. (2001). *The Biological Chemistry of the Elements*, 2nd ed. (Oxford, UK: Clarendon Press).
- Haydon, M.J., and Cobbett, C.S. (2007a). Transporters of ligands for essential metal ions in plants. *New Phytol.* **174**: 499–506.
- Haydon, M.J., and Cobbett, C.S. (2007b). A novel major facilitator superfamily protein at the tonoplast influences zinc tolerance and accumulation in Arabidopsis. *Plant Physiol.* **143**: 1705–1719.
- Higuchi, K., Suzuki, K., Nakanishi, H., Yamaguchi, H., Nishizawa, N.K., and Mori, S. (1999). Cloning of nicotianamine synthase genes, novel genes involved in the biosynthesis of phytosiderophores. *Plant Physiol.* **119**: 471–480.
- Hussain, D., Haydon, M.J., Wang, Y., Wong, E., Sherson, S.M., Young, J., Camakaris, J., Harper, J.F., and Cobbett, C.S. (2004). P-type ATPase heavy metal transporters with roles in essential zinc homeostasis in *Arabidopsis*. *Plant Cell* **16**: 1327–1339.
- Jaquinod, M., Villiers, F., Kieffer-Jaquinod, S., Hugouvieux, V., Bruley, C., Garin, J., and Bourguignon, J. (2007). A proteomics

- dissection of *Arabidopsis thaliana* vacuoles isolated from cell culture. *Mol. Cell. Proteomics* **6**: 394–412.
- Kawachi, M., Kobae, Y., Mimura, T., and Maeshima, M.** (2008). Deletion of a histidine-rich loop of AtMTP1, a vacuolar Zn(2+)/H(+) antiporter of *Arabidopsis thaliana*, stimulates the transport activity. *J. Biol. Chem.* **283**: 8374–8383.
- Kim, S.A., Punshon, T., Lanzirotti, A., Li, L., Alonso, J.M., Ecker, J.R., Kaplan, J., and Guerinot, M.L.** (2006). Localization of iron in *Arabidopsis* seed requires the vacuolar membrane transporter VIT1. *Science* **314**: 1295–1298.
- Klatte, M., Schuler, M., Wirtz, M., Fink-Straube, C., Hell, R., and Bauer, P.** (2009). The analysis of *Arabidopsis* nicotianamine synthase mutants reveals functions for nicotianamine in seed iron loading and iron deficiency responses. *Plant Physiol.* **150**: 257–271.
- Kobae, Y., Uemura, T., Sato, M.H., Ohnishi, M., Mimura, T., Nakagawa, T., and Maeshima, M.** (2004). Zinc transporter of *Arabidopsis thaliana* AtMTP1 is localized to vacuolar membranes and implicated in zinc homeostasis. *Plant Cell Physiol.* **45**: 1749–1758.
- Lanquar, V., Lelièvre, F., Bolte, S., Hamès, C., Alcon, C., Neumann, D., Vansuyt, G., Curie, C., Schröder, A., Krämer, U., Barbier-Brygoo, H., and Thomine, S.** (2005). Mobilization of vacuolar iron by AtNRAMP3 and AtNRAMP4 is essential for seed germination on low iron. *EMBO J.* **24**: 4041–4051.
- Lanquar, V., Ramos, M.S., Lelièvre, F., Barbier-Brygoo, H., Krieger-Liszak, A., Krämer, U., and Thomine, S.** (2010). Export of vacuolar manganese by AtNRAMP3 and AtNRAMP4 is required for optimal photosynthesis and growth under manganese deficiency. *Plant Physiol.* **152**: 1986–1999.
- Lee, S., Jeon, U.S., Lee, S.J., Kim, Y.K., Persson, D.P., Husted, S., Schjørring, J.K., Kakei, Y., Masuda, H., Nishizawa, N.K., and An, G.** (2009). Iron fortification of rice seeds through activation of the nicotianamine synthase gene. *Proc. Natl. Acad. Sci. USA* **106**: 22014–22019.
- Le Jean, M., Schikora, A., Mari, S., Briat, J.F., and Curie, C.** (2005). A loss-of-function mutation in AtYSL1 reveals its role in iron and nicotianamine seed loading. *Plant J.* **44**: 769–782.
- Long, T.A., Tsukagoshi, H., Busch, W., Lahner, B., Salt, D.E., and Benfey, P.N.** (2010). The bHLH transcription factor POPEYE regulates response to iron deficiency in *Arabidopsis* roots. *Plant Cell* **22**: 2219–2236.
- Morrissey, J., Baxter, I.R., Lee, J., Li, L., Lahner, B., Grotz, N., Kaplan, J., Salt, D.E., and Guerinot, M.L.** (2009). The ferroportin metal efflux proteins function in iron and cobalt homeostasis in *Arabidopsis*. *Plant Cell* **21**: 3326–3338.
- Niedenthal, R.K., Riles, L., Johnston, M., and Hegemann, J.H.** (1996). Green fluorescent protein as a marker for gene expression and subcellular localization in budding yeast. *Yeast* **12**: 773–786.
- Nozoye, T., Nagasaka, S., Kobayashi, T., Takahashi, M., Sato, Y., Sato, Y., Uozumi, N., Nakanishi, H., and Nishizawa, N.K.** (2011). Phytosiderophore efflux transporters are crucial for iron acquisition in graminaceous plants. *J. Biol. Chem.* **286**: 5446–5454.
- Outten, C.E., and O'Halloran, T.V.** (2001). Femtomolar sensitivity of metalloregulatory proteins controlling zinc homeostasis. *Science* **292**: 2488–2492.
- Palmer, C.M., and Guerinot, M.L.** (2009). Facing the challenges of Cu, Fe and Zn homeostasis in plants. *Nat. Chem. Biol.* **5**: 333–340.
- Pich, A., Hillmer, S., Manteuffel, R., and Scholz, G.** (1997). First immunohistochemical localization of the endogenous Fe²⁺-chelator nicotianamine. *J. Exp. Bot.* **48**: 759–767.
- Pich, A., Manteuffel, R., Hillmer, S., Scholz, G., and Schmidt, W.** (2001). Fe homeostasis in plant cells: Does nicotianamine play multiple roles in the regulation of cytoplasmic Fe concentration? *Planta* **213**: 967–976.
- Pilon, M., Cohu, C.M., Ravet, K., Abdel-Ghany, S.E., and Gaymard, F.** (2009). Essential transition metal homeostasis in plants. *Curr. Opin. Plant Biol.* **12**: 347–357.
- Porra, R.J., Thompson, W.A., and Kriedemann, P.E.** (1989). Determination of accurate extinction coefficients and simultaneous equations for assaying chlorophylls a and b extracted with four different solvents: Verification of the concentration of chlorophyll standards by atomic absorption spectroscopy. *Biochim. Biophys. Acta* **975**: 384–389.
- Rellán-Álvarez, R., Abadía, J., and Alvarez-Fernández, A.** (2008). Formation of metal-nicotianamine complexes as affected by pH, ligand exchange with citrate and metal exchange. A study by electrospray ionization time-of-flight mass spectrometry. *Rapid Commun. Mass Spectrom.* **22**: 1553–1562.
- Resing, S.A., et al.** (2008). The *Physcomitrella* genome reveals evolutionary insights into the conquest of land by plants. *Science* **319**: 64–69.
- Ricachenevsky, F.K., Sperotto, R.A., Menguer, P.K., Sperb, E.R., Lopes, K.L., and Fett, J.P.** (2011). ZINC-INDUCED FACILITATOR-LIKE family in plants: lineage-specific expansion in monocotyledons and conserved genomic and expression features among rice (*Oryza sativa*) paralogs. *BMC Plant Biol.* **11**: 20.
- Rogers, E.E., and Guerinot, M.L.** (2002). FRD3, a member of the multidrug and toxin efflux family, controls iron deficiency responses in *Arabidopsis*. *Plant Cell* **14**: 1787–1799.
- Schaaf, G., Honsbein, A., Meda, A.R., Kirchner, S., Wipf, D., and von Wirén, N.** (2006). *AtIREG2* encodes a tonoplast transport protein involved in iron-dependent nickel detoxification in *Arabidopsis thaliana* roots. *J. Biol. Chem.* **281**: 25532–25540.
- Schaaf, G., Ludewig, U., Erenoglu, B.E., Mori, S., Kitahara, T., and von Wirén, N.** (2004). ZmYS1 functions as a proton-coupled symporter for phytosiderophore- and nicotianamine-chelated metals. *J. Biol. Chem.* **279**: 9091–9096.
- Shimizu, E., Hayashi, A., Takahashi, R., Aoyagi, Y., Murakami, T., and Kimoto, K.** (1999). Effects of angiotensin I-converting enzyme inhibitor from *Ashitaba* (*Angelica keiskei*) on blood pressure of spontaneously hypertensive rats. *J. Nutr. Sci. Vitaminol. (Tokyo)* **45**: 375–383.
- Simm, C., Lahner, B., Salt, D., LeFurgey, A., Ingram, P., Yandell, B., and Eide, D.J.** (2007). *Saccharomyces cerevisiae* vacuole in zinc storage and intracellular zinc distribution. *Eukaryot. Cell* **6**: 1166–1177.
- Sinclair, S.A., Sherson, S.M., Jarvis, R., Camakaris, J., and Cobbett, C.S.** (2007). The use of the zinc-fluorophore, Zinpyr-1, in the study of zinc homeostasis in *Arabidopsis* roots. *New Phytol.* **174**: 39–45.
- Stephan, U.W., and Scholz, G.** (1993). Nicotianamine: Mediator of transport of iron and heavy metals in the phloem? *Physiol. Plant.* **88**: 522–529.
- Takahashi, M., Terada, Y., Nakai, I., Nakanishi, H., Yoshimura, E., Mori, S., and Nishizawa, N.K.** (2003). Role of nicotianamine in the intracellular delivery of metals and plant reproductive development. *Plant Cell* **15**: 1263–1280.
- Talke, I.N., Hanikenne, M., and Krämer, U.** (2006). Zinc-dependent global transcriptional control, transcriptional deregulation, and higher gene copy number for genes in metal homeostasis of the hyperaccumulator *Arabidopsis halleri*. *Plant Physiol.* **142**: 148–167.
- Trampczynska, A., Böttcher, C., and Clemens, S.** (2006). The transition metal chelator nicotianamine is synthesized by filamentous fungi. *FEBS Lett.* **580**: 3173–3178.
- Trampczynska, A., Küpper, H., Meyer-Klaucke, W., Schmidt, H., and Clemens, S.** (2010). Nicotianamine forms complexes with Zn(II) *in vivo*. *Metallomics* **2**: 57–66.
- Vallee, B.L., and Auld, D.S.** (1990). Zinc coordination, function, and

- structure of zinc enzymes and other proteins. *Biochemistry* **29**: 5647–5659.
- Vandesompele, J., De Preter, K., Pattyn, F., Poppe, B., Van Roy, N., De Paepe A., and Speleman F.** (2002). Accurate normalization of real-time RT-PCR data by geometric averaging of multiple internal control genes. *Genome Biol.* **3**: RESEARCH0034.
- Varotto, C., Maiwald, D., Pesaresi, P., Jahns, P., Salamini, F., and Leister, D.** (2002). The metal ion transporter IRT1 is necessary for iron homeostasis and efficient photosynthesis in *Arabidopsis thaliana*. *Plant J.* **31**: 589–599.
- Vert, G., Grotz, N., Dédaldéchamp, F., Gaymard, F., Guerinot, M.L., Briat, J.F., and Curie, C.** (2002). IRT1, an Arabidopsis transporter essential for iron uptake from the soil and for plant growth. *Plant Cell* **14**: 1223–1233.
- von Wirén, N., Klair, S., Bansal, S., Briat, J.F., Khodr, H., Shioiri, T., Leigh, R.A., and Hider, R.C.** (1999). Nicotianamine chelates both Fe(III) and Fe(II). Implications for metal transport in plants. *Plant Physiol.* **119**: 1107–1114.
- Waters, B.M., Chu, H.H., Didonato, R.J., Roberts, L.A., Easley, R.B., Lahner, B., Salt, D.E., and Walker, E.L.** (2006). Mutations in *Arabidopsis yellow stripe-like1* and *yellow stripe-like3* reveal their roles in metal ion homeostasis and loading of metal ions in seeds. *Plant Physiol.* **141**: 1446–1458.
- Weber, M., Harada, E., Vess, C., Roepenack-Lahaye, E., and Clemens, S.** (2004). Comparative microarray analysis of *Arabidopsis thaliana* and *Arabidopsis halleri* roots identifies nicotianamine synthase, a ZIP transporter and other genes as potential metal hyper-accumulation factors. *Plant J.* **37**: 269–281.
- Yang, T.J., Lin, W.D., and Schmidt, W.** (2010). Transcriptional profiling of the Arabidopsis iron deficiency response reveals conserved transition metal homeostasis networks. *Plant Physiol.* **152**: 2130–2141.
- Yi, Y., and Guerinot, M.L.** (1996). Genetic evidence that induction of root Fe(III) chelate reductase activity is necessary for iron uptake under iron deficiency. *Plant J.* **10**: 835–844.
- Zheng, L., Cheng, Z., Ai, C., Jiang, X., Bei, X., Zheng, Y., Glahn, R.P., Welch, R.M., Miller, D.D., Lei, X.G., and Shou, H.** (2010). Nicotianamine, a novel enhancer of rice iron bioavailability to humans. *PLoS ONE* **5**: e10190.